# Electronic Supplementary Information

# Manipulating the morphology of the nano oxide domain in AuCu-Iron oxide dumbbell-like nanocomposites as a tool to modify magnetic properties

*Sharif Najafishirtari[a], Aidin Lak[b], Clara Guglieri[c], Sergio Marras,[d] Rosaria Brescia[e], Sergio Fiorito[b,f], Elaheh Sadrollahi[g], Fred Jochen Litterst[g], Teresa Pellegrino[b], Liberato Manna[a], Massimo Colombo[a*]*

[a] Nanochemistry Department, Istituto Italiano di Tecnologia, Via Morego 30, 16163 Genoa, Italy.

[b] Nanomaterials for Biomedical Applications, Istituto Italiano di Tecnologia, Via Morego 30, 16163 Genoa, Italy.

[c] Sincrotrone Trieste, ELETTRA, 34012 Basovizza (TS), Italy.

[d] Materials Characterization Facility, Istituto Italiano di Tecnologia, Genoa, 16163, Italy.

[e] Electron Microscopy Facility, Istituto Italiano di Tecnologia, Genoa, 16163, Italy.

[f] Università degli Studi di Genova, Via Dodecaneso, 31, 16146, Genoa, Italy.

[g] Institut für Physik der Kondensierten Materie, Technische Universität Braunschweig, 38106 Braunschweig, Germany.

**Corresponding author: massimo.colombo@iit.it*

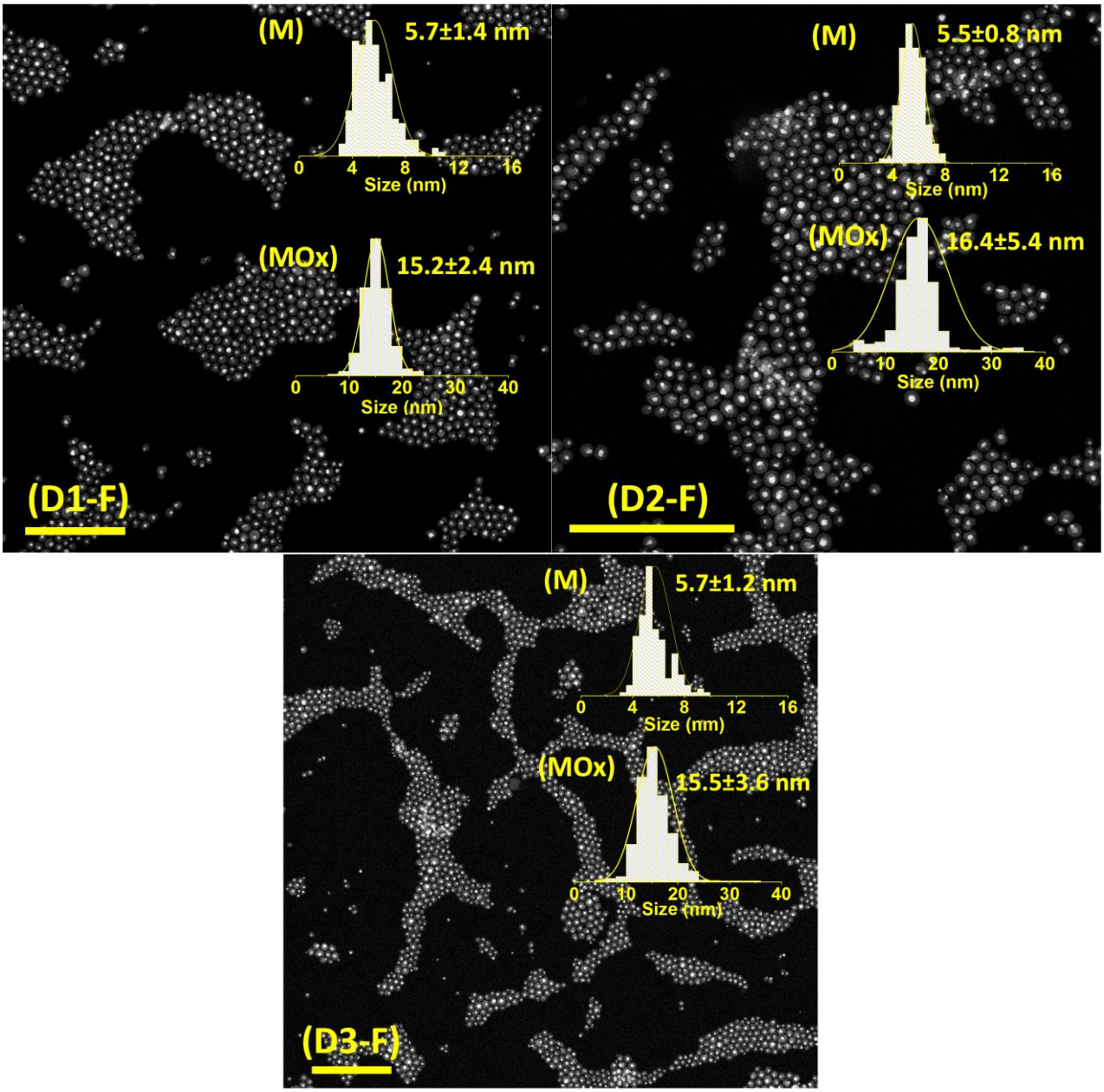


**Figure S1**. Overview of the HAADF-STEM images of the NCs and the size distribution of the metal domain (M) and the metal oxide domain (MOx); the scale bars are 200 nm.

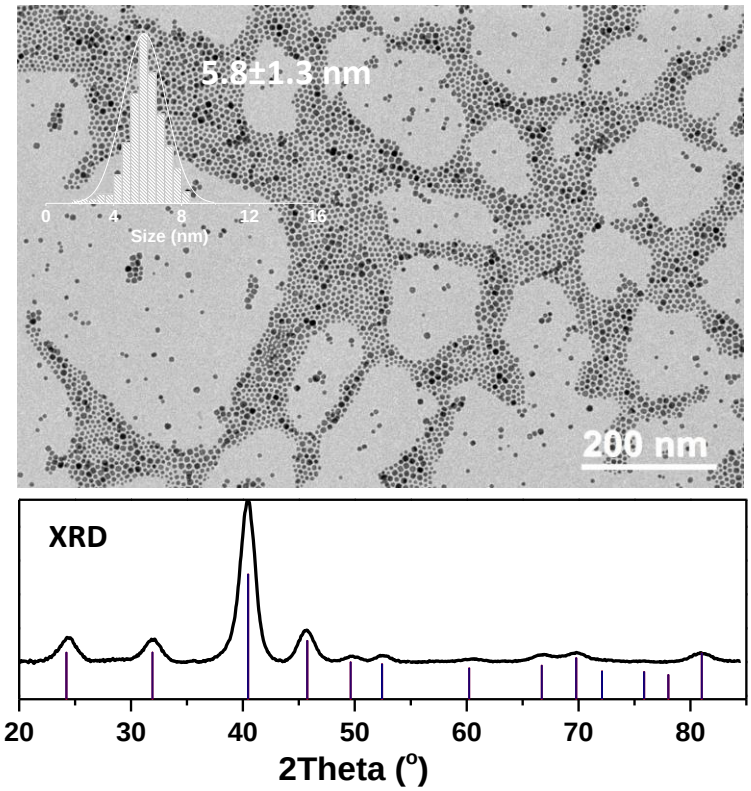


**Figure S2.** Typical bright-field (BF)-TEM image of the as-prepared AuCu colloidal NCs; top left inset: size distribution obtained by measuring ~650 NCs; the XRD pattern of AuCu seeds at the bottom. Experimental data are compared with the database powder XRD pattern for tetragonal AuCu (ICSD code: 42574).

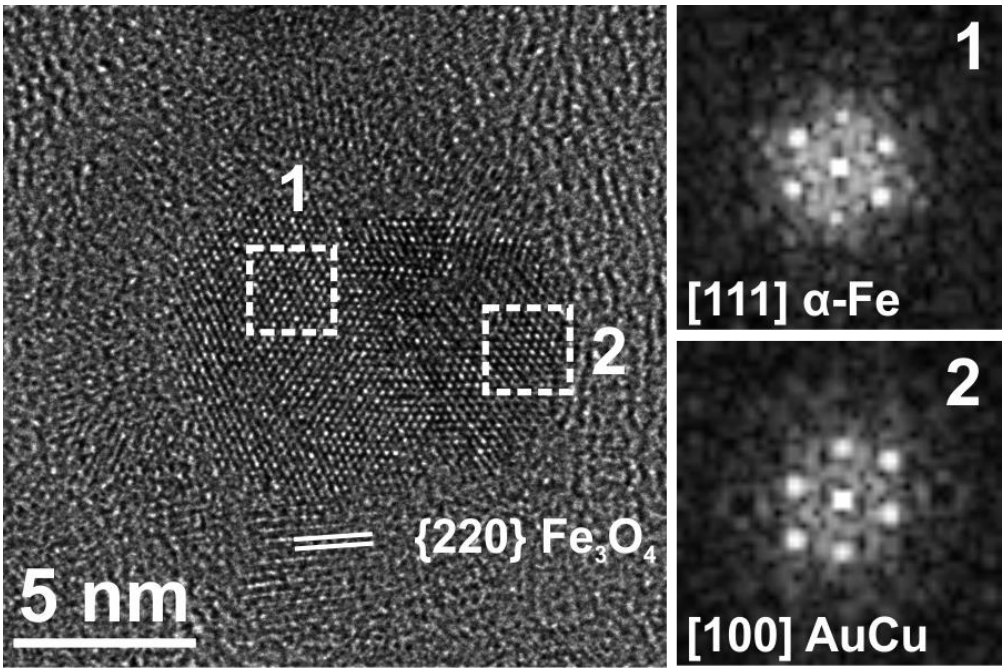


**Figure S3.** HRTEM image of a dumbbell-like NC with an Fe-rich core. The fast Fourier transform of the selected regions can be ascribed to α-Fe (ICSD 52258) and AuCu (tetraauricupride, ICSD 42574), while the periodic fringes in the outer regions of the dumbbell can be ascribed to the $Fe_3O_4$ (magnetite, ICSD 65341), which cannot however be distinguished from the maghemite structure by HRTEM.

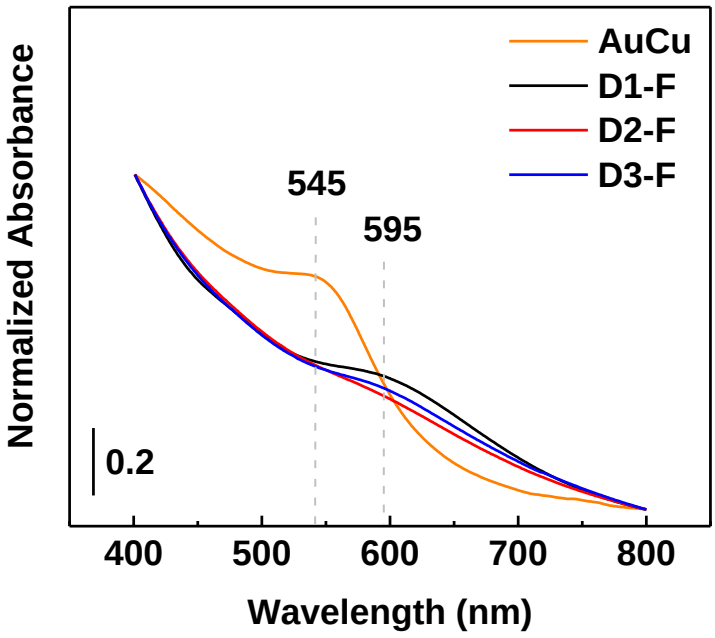


**Figure S4.** Comparison of the normalized absorption spectra for AuCu and the dumbbells. The background spectrum of the solvent was collected before each measurement.

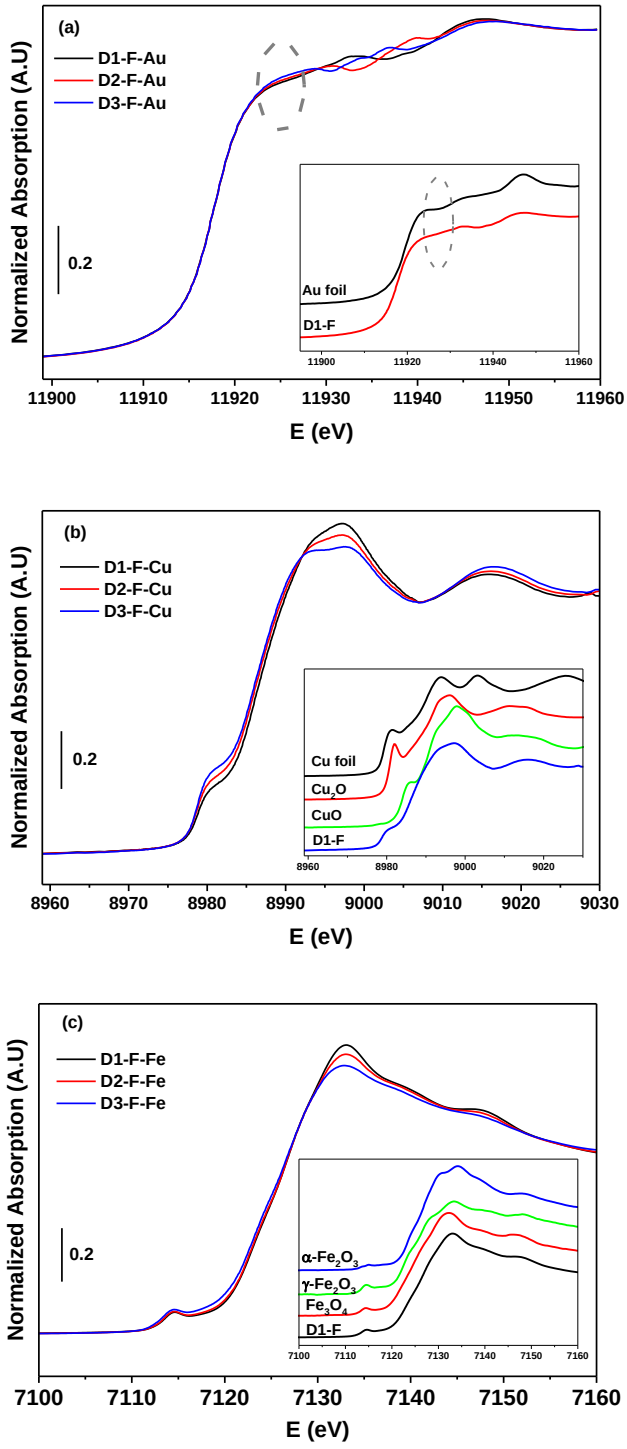


**Figure S5.** XANES spectra of the fresh NCs at different edges of (a ) Au-$L_3$, (b) Cu-K and (c) Fe-K; The reference spectra are shown as insets.

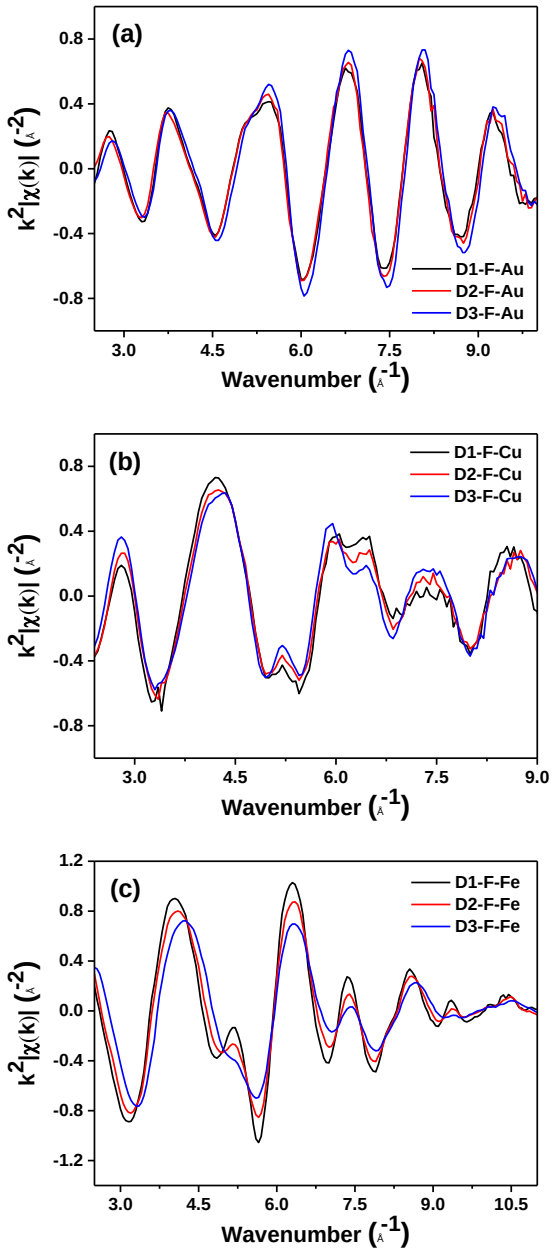


**Figure S6.** $k^2$-weighted EXAFS functions of fresh NCs at different edges of (a) Au-$L_3$, (b) Cu-K and (c) Fe-K.

**The fitting procedure**

With regard to the fitting procedure, crystalline parameters were introduced to the Artemis package using the cluster that was generated around the selected absorbers. The feff sub-routine inside the Demeter package was then operated on the defined clusters to obtain the scattering paths. The $k^2$-weighted EXAFS functions, $k^2\chi(k)$, were then Fourier transformed to isolate the contribution of different scatterings from neighboring atoms as a function of the radial distance, then generally simulated in the selected k ranges considering a number of paths. The selection of the paths was made based on the potential contribution value (in terms of %) provided by the feff sub-routine. Structural parameters were limited to the adjustable parameters of the EXAFS functions, i.e. amplitude reduction factor ($S_0^2$) or the degeneracy of selected path (N) corresponding to each shell, the reference energy ($E_0$), the adjustment of the half path length ($\Delta R$) and the Debye-Waller factor ($\sigma^2$). A full description of the simulation at each edge is given below

**Au edge data:**

Two model clusters were initially constructed around the Au absorbers with respect to the structural data of the AuCu-ICSD code: 42574 in addition to the Au-ICSD Code: 163723 as the present phases in the system. Once the scattering paths had been generated by the software for each phase, a number of them within the Radial distance range of 1.0-4.0 were included in the modelling. The degeneracy of the considered paths was assumed to be the equivalent to that of the model. Then the EXAFS was simulated by assuming a different $S_0^2$ to account for the contributions from the two phases in the EXAFS (see section 13.3 of the reference [1] to account for the mixed phases). The $E_0$ was assumed to be adjustable but similar for all paths in the fitting. Two adjustable $\sigma^2$ were considered in the fitting, corresponding to the Au and Cu elements. The $\Delta R$ parameter in the alloy phase was considered to be different for Au and Cu shells to account for the possible disordered nature of the alloy phase, while another $\Delta R$ was adjusted for the Au shells in the Au phase. The ratio of the number of adjustable variables to the independent data point was 0.55 in this case. At the end, the coordination number at each shell was calculated and reported in Table S2 from the product of N and $S_0^2$ along with the R and $\sigma^2$ corresponding to each shell.

**Cu edge data:**

In this case, two model clusters were initially constructed around the Cu absorbers with respect to the structural data of the AuCu-ICSD code: 42574 in addition to the $Cu_2O$-ICSD Code: 53332 as the present phases in the system. Once the scattering paths had been generated by the software for each phase, a number of them within the Radial distance range of 1.1-4.0 were included for the modelling. The degeneracy of the considered paths was assumed to be the equivalent to that of the model. A similar strategy was applied to account for the contribution of the two phases. The ratio of the number of adjustable variables to the independent data point was 0.61.

**Fe edge data:**

In this case, two model clusters were initially constructed around the Fe absorbers with respect to the structural data of the Magnetite-ICSD code: 65341in addition to the Iron-ICSD Code: 53451. Since the Fe absorbers in the cubic spinel structure of the magnetite/maghemite could be placed at both octahedral and tetrahedral positions, the scattering paths were constructed considering these two types of absorbers in the magnetite structure. Once all paths had been constructed, a number of them within the Radial distance range of 1.1-4.0were considered for the modelling. The degeneracy of the considered paths was assumed to be the equivalent to that of the model. EXAFS was then simulated by assuming a different $S_0^2$ to account for the contributions from the different types of absorbers in the system (i.e. Fe at the octahedral positions in the magnetite, Fe at the tetrahedral positions in the magnetite and in one case also Fe shells in the α-iron phase). The ratio of tetrahedral to octahedral contribution was constrained with respect to the structural data of the model cluster. The $E_0$ was assumed to be adjustable but similar for all paths in the fitting. Two separate adjustable $\sigma^2$ parameters were considered in the fitting, one corresponding to the Fe scatterers and the other to the O ones. For each type of absorber, a different $\Delta R$ adjustment factor assuming an isotropic expansion/contraction was considered for each type of shell in order to account for the highly distorted nature of the system. The ratio of the number of adjustable variables to the independent data point was 0.52 in this case.

**Table S1.** The results of the EXAFS fitting at the Au $L_3$-edge for the fresh samples (k range for the Fourier transform 2.5-10.2 $Å^{-1}$; the R-range for the fitting was 1-4 Å).

| Sample | Scattering Path | CN | R (Å) | $\sigma^2$ | R-factor |
|---|---|---|---|---|---|
| | **AuCu phase** | | | | |
| | Au-Cu1 | 2.72±0.84 | 2.68±0.02 | 0.008±0.003 | |
| | Au-Au1 | 1.36±0.42 | 2.66±0.08 | 0.008±0.004 | |
| | Au-Au2 | 0.68±0.21 | 3.52±0.08 | 0.008±0.004 | |
| **D1-F** | Au-Au3 | 1.36±0.42 | 3.82±0.08 | 0.008±0.004 | 0.027 |
| | **Au phase** | | | | |
| | Au-Au1 | 4.88±1.80 | 2.83±0.03 | 0.008±0.004 | |
| | Au-Au2 | 2.44±0.90 | 4.02±0.03 | 0.008±0.004 | |
| | **AuCu phase** | | | | |
| | Au-Cu1 | 2.96±0.72 | 2.67±0.02 | 0.008±0.002 | |
| | Au-Au1 | 1.48±0.36 | 2.65±0.07 | 0.008±0.004 | |
| | Au-Au2 | 0.74±0.18 | 3.52±0.07 | 0.008±0.004 | |
| **D2-F** | Au-Au3 | 1.48±0.36 | 3.81±0.07 | 0.008±0.004 | 0.019 |
| | **Au phase** | | | | |
| | Au-Au1 | 4.44±1.56 | 2.83±0.03 | 0.008±0.004 | |
| | Au-Au2 | 2.22±0.78 | 4.02±0.03 | 0.008±0.004 | |
| | **AuCu phase** | | | | |
| | Au-Cu1 | 3.29±0.70 | 2.67±0.01 | 0.007±0.002 | |
| | Au-Au1 | 1.65±0.35 | 2.65±0.06 | 0.007±0.004 | |
| | Au-Au2 | 0.82±0.17 | 3.52±0.06 | 0.007±0.004 | |
| **D3-F** | Au-Au3 | 1.65±0.35 | 3.81±0.06 | 0.007±0.004 | 0.016 |
| | **Au phase** | | | | |
| | Au-Au1 | 4.22±1.44 | 2.83±0.03 | 0.007±0.004 | |
| | Au-Au2 | 2.11±0.72 | 4.02±0.03 | 0.007±0.004 | |

**Table S2.** The results of the EXAFS fitting at the Cu K-edge for the fresh samples (k range for the Fourier transform 2.6-8.9 $Å^{-1}$; the R-range for the fitting was 1.1-4 Å).

| Sample | Scattering Path | CN | R (Å) | $\sigma^2$ | R-factor |
|---|---|---|---|---|---|
| **D1-F** | **AuCu phase** | | | | 0.016 |
| | Cu-Au1 | 5.12±0.26 | 2.67±0.02 | 0.015±0.002 | |
| | Cu-Cu1 | 2.56±0.13 | 2.60±0.06 | 0.035±0.010 | |
| | Cu-Cu2 | 1.28±0.06 | 3.47±0.06 | 0.035±0.010 | |
| | Cu-Cu3 | 2.56±0.13 | 3.76±0.06 | 0.035±0.010 | |
| | **$Cu_2O$ phase** | | | | |
| | Cu-O1 | 1.44±0.13 | 1.88±0.01 | 0.003* | |
| **D2-F** | **AuCu phase** | | | | 0.009 |
| | Cu-Au1 | 5.84±0.18 | 2.65±0.02 | 0.017±0.002 | |
| | Cu-Cu1 | 2.92±0.09 | 2.61±0.03 | 0.029±0.006 | |
| | Cu-Cu2 | 1.46±0.05 | 3.48±0.03 | 0.029±0.006 | |
| | Cu-Cu3 | 2.92±0.09 | 3.77±0.03 | 0.029±0.006 | |
| | **$Cu_2O$ phase** | | | | |
| | Cu-O1 | 1.08±0.09 | 1.87±0.01 | 0.003* | |
| **D3-F** | **AuCu phase** | | | | 0.018 |
| | Cu-Au1 | 6.40±0.27 | 2.66±0.03 | 0.017±0.003 | |
| | Cu-Cu1 | 3.20±0.14 | 2.61±0.03 | 0.028±0.005 | |
| | Cu-Cu2 | 1.60±0.07 | 3.48±0.03 | 0.028±0.005 | |
| | Cu-Cu3 | 3.20±0.14 | 3.77±0.03 | 0.028±0.005 | |
| | **$Cu_2O$ phase** | | | | |
| | Cu-O1 | 0.80±0.14 | 1.87±0.02 | 0.003* | |

* Parameter fixed in the fitting

**Table S3.** The results of the EXAFS fitting at the Fe K-edge for the fresh samples (k range for the Fourier transform 2.6-11.1 $Å^{-1}$; the R-range for the fitting was 1.1-4 Å).

| Sample | Scattering Path | CN | R (Å) | $\sigma^2$ | R-factor |
|---|---|---|---|---|---|
| D1-F | **Magnetite (Octa)** | | | | 0.016 |
| | $Fe^{octa}$-O1 | 2.76±0.42 | 1.94±0.03 | 0.006±0.002 | |
| | $Fe^{octa}$-$Fe^{octa}$ | 2.76±0.42 | 3.03±0.02 | 0.013±0.002 | |
| | $Fe^{octa}$-$Fe^{tetra}$ | 2.76±0.42 | 3.54±0.02 | 0.013±0.002 | |
| | $Fe^{octa}$-O3 | 2.76±0.42 | 3.73±0.02 | 0.006±0.002 | |
| | **Magnetite (Tetra)** | | | | |
| | $Fe^{tetra}$-O1 | 0.92±0.14 | 2.10±0.09 | 0.006±0.002 | |
| | $Fe^{tetra}$-$Fe^{octa}$ | 2.76±0.42 | 3.41±0.02 | 0.013±0.002 | |
| | $Fe^{tetra}$-O2 | 2.76±0.42 | 3.42±0.02 | 0.006±0.002 | |
| | $Fe^{tetra}$-$Fe^{tetra}$ | 0.92±0.14 | 3.56±0.02 | 0.013±0.002 | |
| D2-F | **Magnetite (Octa)** | | | | 0.020 |
| | $Fe^{octa}$-O1 | 2.52±0.36 | 1.93±0.02 | 0.006±0.002 | |
| | $Fe^{octa}$-$Fe^{octa}$ | 2.52±0.36 | 3.04±0.02 | 0.014±0.002 | |
| | $Fe^{octa}$-$Fe^{tetra}$ | 2.52±0.36 | 3.56±0.02 | 0.014±0.002 | |
| | $Fe^{octa}$-O3 | 2.52±0.36 | 3.75±0.02 | 0.006±0.002 | |
| | **Magnetite (Tetra)** | | | | |
| | $Fe^{tetra}$-O1 | 0.84±0.14 | 2.06±0.11 | 0.006±0.002 | |
| | $Fe^{tetra}$-$Fe^{octa}$ | 2.52±0.42 | 3.38±0.02 | 0.014±0.002 | |
| | $Fe^{tetra}$-O2 | 2.52±0.42 | 3.40±0.02 | 0.006±0.002 | |
| | $Fe^{tetra}$-$Fe^{tetra}$ | 0.84±0.14 | 3.54±0.02 | 0.014±0.002 | |
| D3-F | **Magnetite (Octa)** | | | | 0.023 |
| | $Fe^{octa}$-O1 | 2.10±0.29 | 1.95* | 0.008±0.002 | |
| | $Fe^{octa}$-$Fe^{octa}$ | 2.10±0.29 | 3.02±0.02 | 0.018±0.002 | |
| | $Fe^{octa}$-$Fe^{tetra}$ | 2.10±0.29 | 3.55±0.02 | 0.018±0.002 | |
| | $Fe^{octa}$-O3 | 2.10±0.29 | 3.73±0.02 | 0.008±0.002 | |
| | **Magnetite (Tetra)** | | | | |
| | $Fe^{tetra}$-O1 | 0.68±0.09 | 1.94* | 0.008±0.002 | |
| | $Fe^{tetra}$-$Fe^{octa}$ | 2.04±0.29 | 3.39±0.02 | 0.018±0.002 | |
| | $Fe^{tetra}$-O2 | 2.04±0.29 | 3.40±0.02 | 0.008±0.002 | |
| | $Fe^{tetra}$-$Fe^{tetra}$ | 0.68±0.09 | 3.54±0.02 | 0.018±0.002 | |
| | **α-iron phase** | | | | |
| | Fe-Fe1 | 1.2* | 2.64±0.01 | 0.018±0.002 | |

* Parameter fixed in the fitting

**Table S4.** Mössbauer hyperfine parameters for samples D1-F and D3-F: S center shift vs. α-Fe at room temperature; $B_{hf}$ magnetic hyperfine field; σ standard width of Gaussian field distribution; Q nuclear electric quadrupole splitting.

| **D1-F 250 K** | | | | | |
|---|---|---|---|---|---|
| | S (mm/s) | $B_{hf}$ (T) | σ | Q (mm/s) | rel. area (%) |
| **A** | 0.35(1) | 0 | | 1.05(2) | 36(2) |
| **M1** | 0.53(1) | 43.6(2) | 2.4(2) | 0 | 38(2) |
| **M2** | 0.32(1) | 47.4(2) | 0.8(2) | 0 | 19(2) |
| **M3** | 0.27(1) | 20.6(2) | 1.6(2) | 0 | 8(2) |

| **D3-F 296 K** | | | | | |
|---|---|---|---|---|---|
| | S (mm/s) | $B_{hf}$ (T) | σ | Q (mm/s) | rel. area (%) |
| **A** | 0.35(1) | 0 | | 0.98(2) | 65(2) |
| **M1** | 0.56(1) | 40.2(2) | 3.8(2) | 0 | 15(2) |
| **M2** | 0.29(1) | 44.7(2) | 1.9(2) | 0 | 8(2) |
| **M3** | 0.14(3) | 20.0(2) | 3.2(2) | 0 | 12(2) |

## References

1. Calvin, S., *XAFS for Everyone*. 2013: Taylor & Francis.